Fractal feature of localized electronic states in Fibonacci arrays of Aharonov-Bohm rings

Atsushi Nomata* and Shinkichi Horie
Department of Physics, Faculty of Science, Tokyo University of Science, 1-3 Kagurazaka, Shinjuku-ku, Tokyo 162-8601, Japan
(Received 9 June 2006; revised manuscript received 26 January 2007; published 29 March 2007)

The property of electronic transport in the Fibonacci array of ideal one-dimensional Aharonov-Bohm rings is studied utilizing the Landauer formalism and by analyzing the quantity called "the Fibonacci invariant," which is derived from renormalization-group ideas. In contrast to previous studies, our invariant is not independent of the Fibonacci generation number j in a limited sense despite its expression having the same form as the previous ones. Even so, this "I-function," which is a j-dependent invariant, is shown to preserve its importance in the study of the transport properties of a quasiperiodic system. The line shape of the I-function at $j \geq 15$ exhibits a fractal-like behavior within the transmission rift (i.e., fine transmission gap). This fractal-like behavior of the line shape of the I-function is characterized by a scaling law. Self-similarity appears in the trace of the transmission probability, when the scaling index is in good agreement with the scaling index at another j.

DOI: 10.1103/PhysRevB.75.115130 PACS number(s): 73.23.−b, 73.63.−b, 73.63.Nm, 85.35.Ds

I. INTRODUCTION

Considerable theoretical and experimental efforts have gone into the study of transmission properties in one-dimensional (1D) aperiodic arrays[1–20] since Kohmoto *et al.*[21] presented a pioneering study on the 1D Fibonacci array as a fascinating problem in solid-state physics. One remarkable feature of aperiodic arrays is that all the one-electron eigenstates in them are neither extended nor localized (in the standard meaning) but of an intermediate kind. More precisely, these states called critical states exhibit multifractal properties. The transport properties of electrons associated with critical states has profound implications in applied physics and materials science.[22]

Apart from presenting an attractive topic in itself, the study of nanoscale science in recent years has made it possible to realize exotic quantum devices whose dimensions are much smaller than the characteristic lengths, which are the mean free path and phase-coherence length of an electron. The quantum devices can be fabricated under precise control that provides ideally formed low-dimensional objects with the expected geometry. In ideal quantum devices that are smaller than the characteristic lengths, the electrons are not scattered by impurities or phonons, and they maintain their phase coherence as they ballistically traverse the quantum devices. The transport property in some of the idealized systems, including such quantum devices, is based on the principle of quantum interference, and this transport property can be controlled by the geometrical configuration of the device. A ring-shaped quantum wire called an Aharonov-Bohm ring is one of the quantum devices where the relative phase difference in each arm of the ring is controlled by an external magnetic field. Since Webb *et al.*[23] experimentally verified the Aharonov-Bohm (AB) effect on an AB ring made from a thin film of polycrystalline gold, there have been extensive theoretical and experimental studies on the ring-shaped quantum wire under the framework of the quantum waveguide theory.[24–33] Besides, studies of the transport property controlled by the geometrical configuration of the quantum devices according to the inflation rule have been subjects of extensive research in the past several years.[10,13,15,17–19]

The most salient property of the electronic transport in the Fibonacci array is to exhibit self-similar trace of the transmission probability, which is formed of three bunch structures in the enlarged region of wave number, and to have six cycle for generation number j, which represents the hierarchy of the Fibonacci number, in the region of wave number appearing self-similarity.[3,5,10] However, from the sole viewpoint of the transmission probability, it is difficult to evaluate how the behavior of transport properties appears in any region of wave number. As a powerful tool that can reveal the behavior of the transport property, there is an invariant associated with the aperiodic array; this invariant is obtained by applying the renormalization-group theory to a class of composite rules proposed by Kohmoto *et al.*[1–3] The invariant analysis provides a clear and simple physical picture. Kohmoto *et al.*[3] studied the transmission of electromagnetic waves through Fibonacci dielectric multilayers and indicated that when the invariant I with an initial condition (i.e., $j=0$) attains the maximum value, the transmission spectra at the optical phase length of a layer has a six cycle for the generation number depending on the value of the maximum I. Jin *et al.*[10] studied the electronic transport property in a Fibonacci array of T-stubs by utilizing invariant analysis on the initial condition and pointed out that when the invariant became a constant value, the self-similarity in the trace of the transmission probability appeared in the entire region of the wave number. Nomata *et al.*[19] studied the transport property in a Fibonacci array of AB rings. In this model, the transmission probability coexists with self-similarity and absence of self-similarity depending on the ratio of half-circumferences of AB rings and the region of wave number, although the six cycle for the generation number appears in a region of wave number without self-similarity. The manner in which the aperiodicity in the Fibonacci rule affects transport properties in AB rings in the 1D continuous waveguide model is a puzzle, and the quantity that totally characterizes the transport property of such a Fibonacci array has not been determined. The aim of this paper is to determine the distinction between two kinds of behaviors of the transmission probabil-

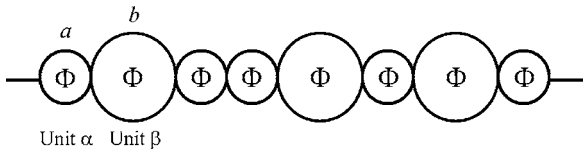

FIG. 1. Schematic diagram of Fibonacci array of AB rings at $j=5$ ($N=8$) comprising units α and β threaded by a magnetic flux Φ. The unit α (β) represents a single AB ring with half-circumference $a(b)$.

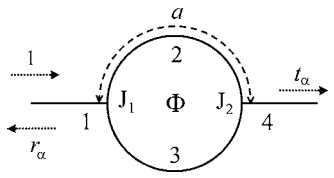

FIG. 2. Schematic diagram of unit α with a half-circumference a threaded by the magnetic flux Φ (i.e., single AB ring). The AB ring is connected to two ideal leads at nodal points J_1 and J_2.

ity, i.e., the appearance of self-similarity and its absence. Thus, we discuss the electronic transport property in the Fibonacci array composed of 1D AB rings by utilizing the invariant analysis.

The outline of this paper is as follows. In Sec. II, we introduce the simple model of a ring-shaped quantum wire reflecting the essence of our problem, and we derive the relevant transfer matrix for the boundary condition in the 1D system. Next, we derive a transfer matrix for an array of rings connected successively according to the Fibonacci rule. We also introduce an invariant in our model in this section. In Sec. III, we present comprehensive numerical results to show the variations of the transmission probability and invariant as a function of the wave number of the incident electron. We also analyze the obtained results in detail. Finally, we summarize our concluding remarks in the last section.

II. THEORY

The model system considered in this paper is a 1D Fibonacci array of AB rings in a 1D quantum wire network, as shown in Fig. 1. This wire network is composed of the units α and β that correspond to AB rings with half-circumferences a and b threaded by a magnetic flux Φ, respectively. The AB rings are connected serially according to the Fibonacci rule $S_{j+1}=\{S_j,S_{j-1}\}$, where j is the generation number, $S_1=\alpha$ and $S_2=\alpha\beta$ [e.g., $S_5=S_4S_3=\alpha\beta\alpha\alpha\beta\alpha\beta\alpha$ (see Fig. 1)]. It is noted that the Fibonacci array of AB rings is *not* translationally invariant. For simplicity, we take the total number of units to be $N=F_j$, where F_j is the Fibonacci number that satisfies $F_{j+1}=F_j+F_{j-1}$ with $F_1=F_0=1$. We assume that the electron is only scattered at the nodal points of two adjacent AB rings.

We utilize the transfer matrix method to obtain the transmission probability for the Fibonacci array of AB rings.[34] If we obtain the transmission and reflection amplitudes for a basic part of the system, we can easily derive a transfer matrix for it and obtain the transmission and reflection amplitudes for the entire system by combining the transfer matrices of all parts of the system. Once we find the transmission amplitude for the entire system, we can easily obtain the transmission probability for it. Thus, we first consider the transmission amplitude for a single AB ring, considering it as a basic part.

Figure 2 shows one of the basic parts of the Fibonacci array of a single AB ring with a half-circumference a (unit α) connected to two ideal leads. To derive the wave functions in this model, we introduce the local coordinate system for the upper and lower arms in Fig. 2 such that the local coordinate direction is taken along the electron-current direction and the origin is taken at the nodal points J_1 and J_2. We assume that the current flows from the left to the right in Fig. 2. The choice of the coordinate origin is noncritical since the interference effect in the AB ring is expressed by the phase factor of wave functions.

In the local coordinate system, the electron motion in the 1D quantum wire subjected to a magnetic field $\boldsymbol{B}(=B\hat{\mathbf{e}}_z)$ perpendicular to the ring plane is governed by the Schrödinger equation[24]

$$\frac{1}{2m^*}\left(-i\hbar\frac{d}{dx}-e\frac{\Phi}{2a}\right)^2\phi(x)=E\phi(x), \tag{1}$$

where $\Phi\equiv f(\Phi_0/2\pi)$ is the magnetic flux through the ring with the quantum unit of flux $\Phi_0\equiv h/e$; f, the flux number corresponding to the magnitude of the magnetic field; e, the electronic charge; $\hbar$, the Dirac constant; and m^*, the effective mass of an electron. Moreover, $\Phi/2a$ corresponds to the vector potential along the AB ring.

In the local coordinate system, wave functions in the regions 1, 2, 3, and 4 in the AB ring can be obtained from Eq. (1) and are written as

$$\begin{aligned}\phi_1(x_1)&=e^{ikx_1}+r_\alpha e^{-ikx_1},\\ \phi_2(x_2)&=C_2e^{ik_{\mathrm{I}}x_2}+D_2e^{-ik_{\mathrm{II}}x_2},\\ \phi_3(x_3)&=C_3e^{ik_{\mathrm{II}}x_3}+D_3e^{-ik_{\mathrm{I}}x_3},\\ \phi_4(x_4)&=t_\alpha e^{ikx_4},\end{aligned} \tag{2}$$

where t_α (r_α) is a transmission (reflection) amplitude, while C_2 (D_2) and C_3 (D_3) are the amplitudes of wave functions in regions 2 and 3, respectively. k denotes the wave number of the incident electron having energy $E=\hbar^2k^2/2m^*$. It is noted that in regions 1 and 4 the magnetic flux Φ is zero. Here, we assumed that k_{I} is the wave number of an electron moving along the vector potential direction and k_{II} is the wave number of an electron moving along the opposite direction in regions 2 and 3 (i.e., the upper and lower arms in Fig. 2). The wave numbers k_{I} and k_{II} are given by $k_{\mathrm{I}}=k+f/(2a)$ and $k_{\mathrm{II}}=k-f/(2a)$, respectively.

The transmission and reflection amplitudes can be determined simply by matching the boundary conditions for these wave functions. Utilizing Griffith's boundary conditions[35] at nodal points J_1 and J_2, the continuity of the wave functions and the conservation of current density are ensured at these

nodal points. The transmission and reflection amplitudes for unit α are, respectively, given by

$$t_\alpha = \frac{16i}{\Delta_S(k,f,a)} \sin ka \cos\frac{f}{2}, \tag{3}$$

$$r_\alpha = \frac{1}{\Delta_S(k,f,a)}(2 - 4\cos f - 3\cos 2ka), \tag{4}$$

where a is the half-circumference of the AB ring and $\Delta_S(k,f,a)$ is given by $\Delta_S(k,f,a) \equiv 2 + 8\cos f - 9e^{-2ika} - e^{2ika}$.

The transfer matrix $\boldsymbol{M}_\alpha$ for unit α is expressed by

$$\boldsymbol{M}_\alpha = \begin{pmatrix} 1/t_\alpha^* & -r_\alpha^*/t_\alpha^* \\ -r_\alpha/t_\alpha & 1/t_\alpha \end{pmatrix}, \tag{5}$$

where the asterisk denotes the complex conjugate. We can also obtain the transfer matrix $\boldsymbol{M}_\beta$ for a single AB ring with a half-circumference b (unit β) in a similar manner. The total transfer matrix is given by the product of the transfer matrices of all the basic parts according to the arrangement rule for the Fibonacci array.

The transfer matrix $\boldsymbol{M}_{j+1}$ for the $(j+1)$th Fibonacci array is given by a composite rule as follows:

$$\boldsymbol{M}_{j+1} = \boldsymbol{M}_j \boldsymbol{M}_{j-1} \quad (j \geq 1), \tag{6}$$

where $\boldsymbol{M}_0 = \boldsymbol{M}_\beta$ and $\boldsymbol{M}_1 = \boldsymbol{M}_\alpha$. This composite rule corresponds to the Fibonacci rule. It is noted that the total number N of AB rings in this array corresponds to the Fibonacci number. The transfer matrix for the N-connected Fibonacci array can be expressed by

$$\boldsymbol{M}_N = \begin{pmatrix} 1/t_N^* & -r_N^*/t_N^* \\ -r_N/t_N & 1/t_N \end{pmatrix}, \tag{7}$$

where t_N is the total transmission amplitude and r_N is the total reflection amplitude. The total transmission probability for the N-connected Fibonacci array is finally obtained by $T_N = t_N^* t_N$. The two-terminal conductance of the entire system at the zero temperature is obtained by the Landauer formula $G_N = (2e^2/h)T_N$.[36]

Next, we will obtain an invariant for the Fibonacci array of AB rings by applying renormalization-group ideas. The composite rule in Eq. (6) also provides a powerful calculational scheme since the rule can be regarded as a kind of renormalization-group equation depending on dynamical systems determined by the initial conditions $\boldsymbol{M}_0 = \boldsymbol{M}_\beta$ and $\boldsymbol{M}_1 = \boldsymbol{M}_\alpha$.[1–3,21] The deduced renormalization-group equation is as follows:

$$x_{j+1} = 2x_j x_{j-1} - x_{j-2}, \tag{8}$$

where $x_j = \frac{1}{2}\,\mathrm{Tr}\,\boldsymbol{M}_j$. The initial condition for this dynamical system can be taken as

$$x_0 = \frac{1}{2}\,\mathrm{Tr}\,\boldsymbol{M}_\beta = \frac{\cos kb}{\cos(f/2)},$$

$$x_1 = \frac{1}{2}\,\mathrm{Tr}\,\boldsymbol{M}_\alpha = \frac{\cos ka}{\cos(f/2)},$$

$$x_{-1} = \frac{1}{2}\,\mathrm{Tr}[\boldsymbol{M}_\beta \boldsymbol{M}_\alpha^{-1}]$$

$$= \frac{1}{4\sin ka \sin kb \cos^2(f/2)} \times [2\cos^2 k(a-b) - 2\cos k(a+b) \times \cos k(a-b)\cos^2(f/2) + \cos f - 1]. \tag{9}$$

Furthermore, Kohmoto *et al.* defined the three-dimensional space spanned by $\boldsymbol{r}_j = (x_j, x_{j+1}, x_{j+2})$ and related Eq. (8) to the mapping from $\boldsymbol{r}_j$ to $\boldsymbol{r}_{j+1}$. The orbit $\{\boldsymbol{r}_j\}$ is confined on a two-dimensional manifold determined by an invariant[2,21] given by

$$I = x_{j-1}^2 + x_j^2 + x_{j+1}^2 - 2x_{j-1}x_j x_{j+1} - 1. \tag{10}$$

We consider that the expression in Eq. (8) can be applied in our model since the expression is determined by the composite rule in Eq. (6). Substituting Eq. (9) into Eq. (10), the explicit expression of the invariant at $j=0$ is given by

$$I = \frac{1}{\cos^2(f/2)}\{\cos^2 ka + \cos^2 kb\} + \frac{D(k,f,a,b)}{16\sin^2 ka \sin^2 kb \cos^4(f/2)} \times [D(k,f,a,b) - 2\sin 2ka \sin 2kb] - 1, \tag{11}$$

where $D(k,f,a,b) \equiv 2\cos^2 k(a-b) - 2\cos^2(f/2)\cos k(a+b)\cos k(a-b) + \cos f - 1$. By substituting Eq. (8) directly in Eq. (10), one can see that this invariant is indeed independent of j.

However, here we argue that this is not the case for our I. The invariant I for the tight-binding model proposed by Kohmoto *et al.* is determined by the difference between two values of the potential (hopping matrix elements); therefore, the potential is a key parameter to maintain I as an invariant under the renormalization-group transformation.[2,21] However, the invariant for our model is determined by the half-circumference of rings, wave number k, and magnetic flux number f. Thus, I for the tight-binding model is parametrized by the potential difference only, whereas I for our model has two extra parameters, k and f, besides the ratio of the half-circumferences. This multiparameter nature makes our I with higher j different from Eq. (11) in a limited sense. We explain our argument. Each matrix element of our transfer matrix $\boldsymbol{M}_j$ [Eq. (7)] is a function of the wave number k and the magnetic flux number f. Due to the fact that the presence of a magnetic flux breaks the time-reversal symmetry of the system,[37–39] electron state antiresonance can occur and the transmission amplitude t_j (and also its complex conjugate) may then become zero. Hence, each matrix element of $\boldsymbol{M}_j$ may have some singularities on the k axis, at each of which not only the matrix element but also x_j diverges. The number of singularities varies depending on f and j. Each singularity moves as f varies and j increases. Both these singular features of $\boldsymbol{M}_j$ are associated with the electronic properties of the present system, such as the transmission probability. The introduction of singularities in the matrix elements provides

invariant I with a j dependency. If a singularity is hidden at a low value of j, I behaves as if it is an invariant; on the other hand, a higher j exposes that singularity and I then depends on j. When each matrix element has no singularity at the initial condition, I remains an invariant even at high values of j. We assert that while almost all the other systems, including the tight-binding model studied previously, do not have such matrices with singularities, there are some other systems with a j-dependent I that are different from the present one.[40] Thus, to distinguish between previous forms of I and the j-dependent invariant, we refer to the latter as "I-function" in the discussion below. At first glance, this j dependency of I (I-function) appears to be a negative feature in the study of the characteristic properties of quasiperiodic systems. The importance of the I-function lies in the fact that it is independent of j. Nevertheless, the I-function is a powerful tool to study the electronic properties of the system under consideration. This will be shown in the following section.

III. RESULTS AND DISCUSSION

In this section, we present the numerical results of the transmission probability and I-function as a function of k/π. First, we discuss the transmission properties for a single ring and double ring at $f=0$. After comparing the transmission probability in a single ring with that in a double ring, we present the transmission probability in Fibonacci arrays of rings at $f=0$ by utilizing the invariant (I-function) analysis. Next, we discuss transmission properties in a single AB ring and double AB ring at $f=0.5\pi$. Finally, we present the relationship between the trace of the transmission probability and the line shape of the I-function in the Fibonacci array of AB rings at $f=0.5\pi$. Throughout the numerical calculation, we have confined the half-circumference of AB rings to relatively prime and chosen units where $e=\hbar=2m^*=1$.

A. The case of $f=0$

In the case of a single ring with a half-circumference a at $f=0$, the transmission probability T_S is obtained from Eq. (3) as follows:

$$T_S = \frac{16}{25 - 9\cos^2 ka}, \tag{12}$$

where k is the wave number of an incident electron. T_S oscillates as a function of ka. In the case of $k=n\pi/a$ ($n=0,\pm1,\pm2,\pm3,\ldots$), perfect transmission (i.e., $T_S=1$) occurs in the single ring and the electron travels from region 1 to region 4 smoothly. Here, the wave number satisfies the periodic boundary condition $e^{i2ka}=1$ and standing waves develop in between the nodal points due to this boundary condition.

For double rings with half-circumferences a and b at $f=0$, the transmission probability T_D is derived as

$$T_D = \frac{16}{25 - 9\cos^2 k(a+b)}, \tag{13}$$

utilizing the transfer matrix method.

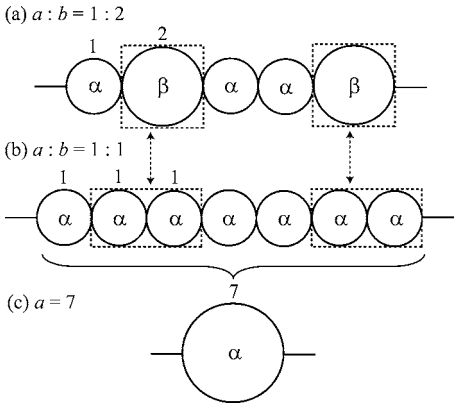

FIG. 3. Schematic diagram of array of rings at $f=0$. (a) Fibonacci, (b) periodic and (c) single ring. The single ring with a half-circumference $b=2$ can be replaced by double rings with a half-circumference $a=1$, and the Fibonacci and periodic arrays of rings can be replaced by a single ring.

Comparing Eq. (12) with Eq. (13), the expression for T_D is identical to the expression for T_S except for the term containing the half-circumference $(a+b)$. Here, we assume that the expression for the transmission probability T_{F_j} in the Fibonacci array is also identical to the expression for T_S except for the term containing the half-circumference as in the case of Eq. (13); the transmission probability T_{F_j} for the Fibonacci array at $f=0$ can be expressed by

$$T_{F_j} = \frac{16}{25 - 9\cos^2 k(aF_j + bF_{j-1})}, \tag{14}$$

where F_j and F_{j-1} are Fibonacci numbers that satisfy $F_{j+1}=F_j+F_{j-1}$ with $F_0=F_1=1$. Indeed, the result of the numerical calculation for the arrangement of rings in Fig. 3 indicates that the trace of T_{F_j} for the Fibonacci array accords fully with the trace of T_S for a single ring.

To elucidate the behavior of the transmission probability T_{F_j} in the Fibonacci array, we apply the invariant (I-function) analysis proposed by Kohmoto *et al.*[2,21]

Substituting $f=0$ into Eq. (9), the initial condition on the mapped dynamical system in Eq. (11) is given by $x_{-1}=\cos k(a-b)$, $x_0=\cos kb$, and $x_1=\cos ka$. From this initial condition, the I-function at $f=0$ becomes zero. In addition, in the case of $a=b$ (i.e., periodic array) and f with an arbitrary flux number, the I-function is again zero from Eq. (11) analytically. This implies that the I-function has no singularity at the initial condition. As mentioned in Sec. II, the absence of a singularity for I ensures that the I-function of the initial condition is sufficient for the analysis. Thus, in the invariant (I-function) analysis we focus on the I-function for the initial condition.

From the above consideration, the zero value of I at $f=0$ can provide a clear and simple physical picture. Figure 3(a) shows the schematic diagram for the Fibonacci array of rings composed of $S_4=\alpha\beta\alpha\alpha\beta$ with $a:b=1:2$. From the invariant (I-function) analysis, all single rings with $b=2$ can be replaced with two single rings with $b=1$ (i.e., the half-circumference of the single ring with $b=2$ is halved), and the

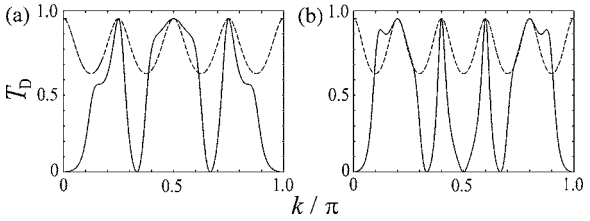

FIG. 4. Transmission probability T_D vs wave number k/π in double AB rings. (a) $a:b=1:3$, (b) $a:b=2:3$. The dashed line is the trace of the transmission probability at $f=0$, while the solid line is the trace at $f=0.5\pi$.

Fibonacci array of rings composed of $S_4=\alpha\beta\alpha\alpha\beta$ with $a:b=1:2$ can be equivalent to a periodic array of seven rings with $a:b=1:1$ [see Fig. 3(b)] and vice versa (i.e., the periodic array with $a:b=1:1$ can be replaced with the Fibonacci array with $a:b=1:2$). Now, from the dividing rule discussed above, the arrangement of rings in Figs. 3(a) and 3(b) can be replaced with a single ring with $a=7$ as shown in Fig. 3(c).

Utilizing the *I*-function analysis for the initial condition, we find that the expression for T_{F_j} in the Fibonacci array of rings is identical to the expression for T_S except for the half-circumference term. Therefore, *the behavior of the transmission probability at* $f=0$ *is independent of the arrangement rule for rings.*

B. The case of $f=0.5\pi$

The transmission probability T_S for a single AB ring at $f=0.5\pi$ is derived from Eq. (3) as follows:

$$T_S = \frac{8\sin^2 ka}{9 - 14\cos^2 ka + 9\cos^4 ka}, \tag{15}$$

T_S at $f=0.5\pi$ oscillates as a function of the period $a\pi$ as in the case of the single ring at $f=0$. As shown in Figs. 4(a) and 4(b), it is characteristic that resonance points (i.e., $T_S=1$) appear in the trace of the transmission probability whenever the wave number k equals $n\pi/a$ $(n=0,\pm1,\pm2,\pm3,\ldots)$ at $f=0$, while antiresonance points (i.e., $T_S=0$) appear in the trace of the transmission probability whenever the wave number k equals $n\pi/a$ at $f=0.5\pi$. The antiresonance at these wave numbers is caused by the breakdown of the time-reversal symmetry.[37–39]

For a double AB ring at $f=0.5\pi$, the transmission probability T_D is derived from the transfer matrix method as follows:

$$T_D = \frac{16\sin^2 ka\sin^2 kb}{\Delta_D(k,a,b)}, \tag{16}$$

where $\Delta_D(k,a,b)$ is given by

$$\begin{aligned}\Delta_D(k,a,b) \equiv\ & 4 - 2\cos k(a+b)\cos k(a-b) + 9\cos^2 k(a+b) \\ & + \cos^2 k(a-b) - 6\cos^3 k(a+b)\cos k(a-b) \\ & + 3\cos^2 k(a+b)\cos^2 k(a-b) - 9\cos^4 k(a+b).\end{aligned}$$

Comparing Eq. (13) with Eq. (16), the transmission probability T_D at $f=0$ does not become zero in the entire region of k, while T_D at $f=0.5\pi$ becomes zero at $k=n\pi/a$ or $k=n\pi/b$. Here, it is noted that the wave numbers for which n/a or n/b is an integer are removed from the entire region of k since the transmission probability approaches infinity at the k values that equal an integral multiple of π. The zero transmission at these wave numbers is caused by the breakdown of the time-reversal symmetry as in the case of a single ring. There are a couple of research works that help in understanding the characteristics of electron flow near the singular points of transmission probabilities in multiply-connected open AB rings.[33]

Figures 4(a) and 4(b) show traces of T_D as a function of k/π for $a:b=1:3$ and $a:b=2:3$, respectively. The solid line represents traces of T_D at $f=0.5\pi$, and the dashed line represents traces of T_D at $f=0$. In the cases where the half-circumferences a and b of AB rings are relatively prime, the transmission probability has the period π in both the periodic and Fibonacci arrays of AB rings.[19] Thus, we discuss only the region $k\in[0,\pi]$ for the double AB ring. As shown in Fig. 4(a) for $a:b=1:3$, the trace of the transmission probability for $f=0.5\pi$ exhibits four dips at $k=\delta\pi$, $\pi/3$, $2\pi/3$, and $(1-\delta)\pi$, and in Fig. 4(b) for $a:b=2:3$ the trace for $f=0.5\pi$ exhibits five dips at $k=\delta\pi$, $\pi/3$, $\pi/2$, $2\pi/3$, and $(1-\delta)\pi$, where δ is a positive infinitesimal quantity. Therefore, the number of dips (i.e., $T_D=0$) for $k\in[0,\pi]$ is given by $(a+b)$. Here, we again notice that a and b are relatively prime.

Next, we discuss the transmission property in a Fibonacci array of rings at $f=0.5\pi$. Figure 5 shows the numerical results of the transmission probability T_{F_j} as a function of k/π. The generation number is fixed at $j=17$ (which corresponds to 2584 units comprising α and β). Figures 5(a) and 5(b) show the traces of the transmission probability for $a:b=1:3$ and $a:b=2:3$, respectively. It is noteworthy that the number of transmission gaps in Fig. 5(a) corresponds to four, $k=\delta\pi$, $\pi/3$, $2\pi/3$, and $(1-\delta)\pi$ for $k\in[0,\pi]$, and the number of transmission gaps in Fig. 5(b) corresponds to five, $k=\delta\pi$, $\pi/3$, $\pi/2$, $2\pi/3$, and $(1-\delta)\pi$ for $k\in[0,\pi]$. Thus, in the Fibonacci array of AB rings, the relationship between the number of AB rings and gaps for $k\in[0,\pi]$ is given by $(a+b)$ as in the case of the double AB ring with $f=0.5\pi$.

In previous works by Jin *et al.*, the electronic transport property in quantum wires with serial T-stubs was studied utilizing the transfer matrix method.[10] They found that the trace of the transmission probability exhibited self-similarity formed of three bunch structures and a six cycle for the generation number j. The transport property in a Fibonacci array composed of AB rings is based on the principle of quantum interference effect as in the case of the Fibonacci array composed of T-stubs. Thus, the feature of self-similarity and the six cycle can be observed in the traces of the transmission probability of the Fibonacci array composed of AB rings.

Figure 5(c) shows the trace of the transmission probability with $a:b=1:3$ in the enlarged region of $0.791\leq k/\pi\leq 0.852$ in Fig. 5(a), and Fig. 5(e) is the trace of the transmission probability in the enlarged region of $0.813\leq k/\pi\leq 0.828$ in Fig. 5(c). Figure 5(d) shows the trace of the transmission probability with $a:b=2:3$ in the enlarged region of $0.823\leq k/\pi\leq 0.898$ in Fig. 5(b), and Fig. 5(f) is the trace of

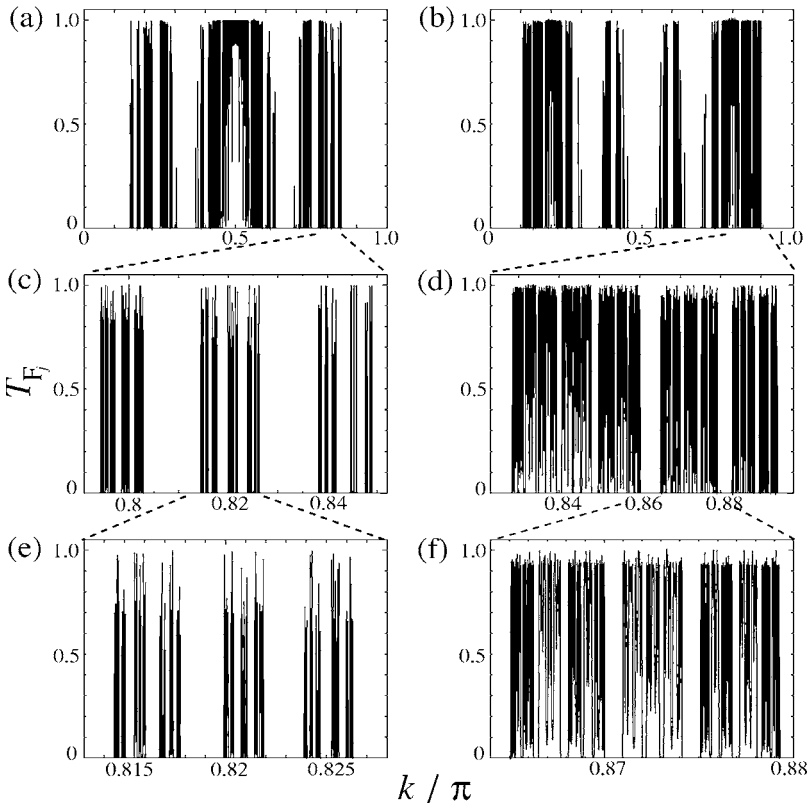

FIG. 5. Transmission probability T_{F_j} vs wave number k/π in Fibonacci array of AB rings at $j=17$ and $f=0.5\pi$. (a) $0\leq k/\pi\leq 1$ with $a:b=1:3$, (b) $0\leq k/\pi\leq 1$ with $a:b=2:3$, (c) $0.791\leq k/\pi\leq 0.852$ with $a:b=1:3$, (d) $0.823\leq k/\pi\leq 0.898$ with $a:b=2:3$, (e) $0.813\leq k/\pi\leq 0.828$ with $a:b=1:3$, and (f) $0.864\leq k/\pi\leq 0.880$ with $a:b=2:3$.

the transmission probability in the enlarged region of $0.864\leq k/\pi\leq 0.880$ in Fig. 5(d). As shown in Figs. 5(c) and 5(e), the traces of transmission probability exhibit self-similarity of three bunch structures. However, Figs. 5(d) and 5(f) do not exhibit self-similarity.

Figure 6 shows traces of the transmission probability at $j=11$, 14, and 17. In Figs. 6(a), 6(c), and 6(e), the ratio of half-circumferences is fixed at $a:b=1:3$, while it is $a:b=2:3$ in Figs. 6(d)–6(f). The trace of the transmission probability in Fig. 6(a) is similar to that in Fig. 6(e), while the trace of the transmission probability in Fig. 6(b) is similar to that in Fig. 6(f); this holds despite the regions k/π in these traces of transmission probability being different from each other. These results of Fig. 6 indicate that the traces of transmission probability exhibit six cycle behavior for the generation number j. Moreover, it is remarkable that six cycle for j appears in the traces of transmission probability *regardless of the appearance of self-similarity*. This result in the transmission behavior indicates that *the six cycle behavior for j is an intrinsic character of the transport property of Fibonacci arrays*. Here, we turn to the I-function analysis. The electronic transport property in the region of transmission minibands is also discussed utilizing the I-function. First, we consider the I-function for the initial condition $j=0$. Substituting $f=0.5\pi$ into Eq. (9), the initial condition for the mapped dynamical system is given by $x_0=\sqrt{2}\cos kb$, $x_1=\sqrt{2}\cos ka$, and $x_{-1}=[2\cos^2 k(a-b)-\cos k(a+b)\cos k(a-b)-1]/(2\sin ka\sin kb)$ at $f=0.5\pi$. Therefore, the I-function for the initial condition at $f=0.5\pi$ is expressed as

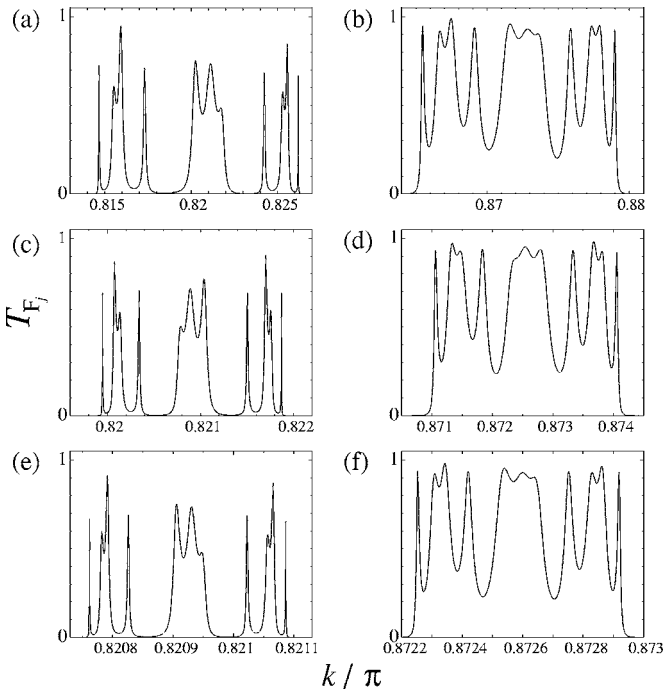

FIG. 6. Transmission probability T_{F_j} vs wave number k/π in Fibonacci array of AB rings at $f=0.5\pi$. The ratio of the half-circumferences of AB rings is $a:b=1:3$ [(a), (c), and (e)] and $a:b=2:3$ [(b), (d), and (f)]. The total numbers of AB rings are (a) and (b) $N=144$ ($j=11$), (c) and (d) $N=610$ ($j=14$), and (e) and (f) $N=2584$ ($j=17$).

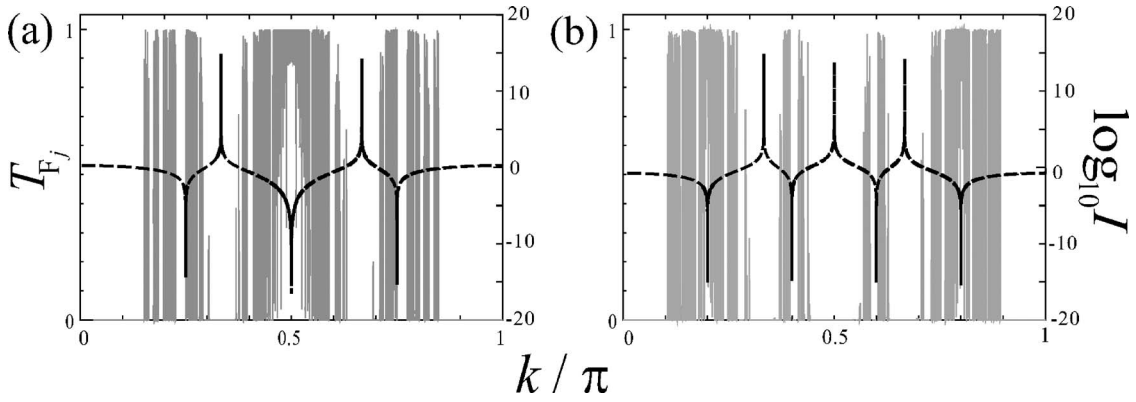

FIG. 7. Transmission probability T_{F_j} and the I-function for the initial condition vs wave number k/π in Fibonacci array of AB rings at $f=0.5\pi$ and $j=17$. The ratio of the half-circumferences of AB rings is $a:b=1:3$ in (a), while it is $a:b=2:3$ in (b). The solid line is the trace of the transmission probability and the dashed line is the line shape of common logarithm of the I-function at $j=0$.

$$I = \frac{1}{4\sin^2 ka \sin^2 kb} \times [1-\cos k(a+b)][1+\cos k(a+b)] \times [1-\cos k(a-b)][1+\cos k(a-b)]. \quad (17)$$

For Eq. (17), the I-function becomes zero at $k=n\pi/(a+b)$ or $k=n\pi/(a-b)$ $(n=0,\pm1,\pm2,\pm3,\ldots)$. In addition, the I-function approaches infinity at $k=n\pi/a$ or $k=n\pi/b$. Figures 7(a) and 7(b) show the traces of transmission probability and the line shape of the I-function as a function of k/π. The dashed lines represent the line shape of the common logarithm of the I-function for the initial condition, while the solid lines represent the traces of transmission probability. The traces of transmission probability in Figs. 7(a) and 7(b) are the same as those in Figs. 5(a) and 5(b).

As shown in Figs. 7(a) and 7(b), each line shape of the I-function exhibits dips approaching −15 in the region of the transmission minibands. The dips in Fig. 7(a) are located at $k=\pi/4$, $\pi/2$, and $3\pi/4$, and those in Fig. 7(b) are located at $k=\pi/5$, $2\pi/5$, $3\pi/5$, and $4\pi/5$. On the other hand, the line shape of the I-function exhibits peaks approaching 15 at $k=\pi/3$ and $2\pi/3$, and the line shape of the I-function in Fig. 7(b) exhibits peaks approaching 15 at $k=\pi/3$, $\pi/2$, and $2\pi/3$. As discussed in the case of the double AB ring at $f=0.5\pi$, the resonance points in $k\in(0,\pi)$ appear in the trace of the transmission probability when the wave number k equals $\pi/4$, $\pi/2$, and $3\pi/4$ with $a:b=1:3$ and $\pi/5$, $2\pi/5$, $3\pi/5$, and $4\pi/5$ with $a:b=2:3$. In addition, the antiresonance points in $k\in(0,\pi)$ appear in the trace of the transmission probability when the wave number k equals $\pi/3$ and $2\pi/3$ with $a:b=1:3$ and $\pi/3$, $\pi/2$, and $2\pi/3$ with $a:b=2:3$. As shown in Figs. 5(a) and 5(b), the transmisson gaps in the Fibonacci array of AB rings are located at the wave number at which the dips appear. We consider that the resonance points in the Fibonacci array of AB rings also correspond to those in double AB rings. Thus, the divergent behavior of the I-function indicates that *the resonance points appear when the line shape of the I-function exhibits dips, while antiresonances* (*the transmission gaps*) *appear when the line shape of the I-function approaches infinity*. There is a research study that investigated the behavior of conductance in relation to the underlying chaotic map and its invariant.[8] Moulopoulos *et al.* analytically provided that resonances occur at special points associated with the vanishing of invariant I of the underlying dynamical map.

In Sec. II, we mentioned that the singular features of $\boldsymbol{M}_j$ are associated with the invariant I with j dependency (I-function), and the line shape of the I-function at a higher j can exhibit peaks within the transmission gaps in the region of the transmission minibands. The Fibonacci system proposed by Kohmoto *et al.* or almost all the other Fibonacci systems studied previously do not have singularities in the matrix elements. In these systems, the I-function is independent of j. Thus, the manner in which the behavior of the I-function in the system having singularities in the matrix elements is characterized by the generation number for $j\neq0$ should be clarified, and it is attractive to study how the line shape of the I-function is affected by the generation number for $j\neq0$. Finally, we discuss the behavior of the I-function by utilizing the I-function analysis for $j\neq0$.

Figure 8 shows the trace of the transmission probability as a function of k/π at $j=10$ (dashed line), and the line shapes of the I-function are shown as a function of k/π at $j=0$ (dotted line) and $j=10$ (solid line). We find two features: (i) The line shape of the I-function at $j=10$ accords with that at $j=0$ in the region of the transmission minibands. (ii) The line shape of the I-function at $j=10$ exhibits peaks unlike that at

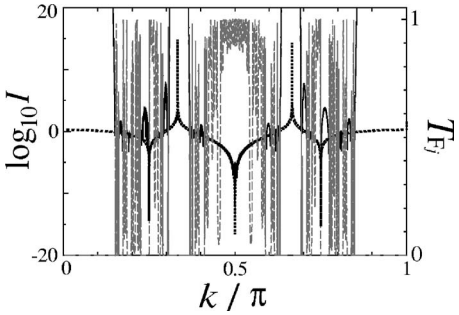

FIG. 8. The I-function $\log_{10} I$ vs wave number k/π in Fibonacci array of AB rings at $f=0.5\pi$, $a:b=1:3$. (a) The dashed line is the trace of T_{F_j} at $j=10$. The dotted and solid lines are line shapes of $\log_{10} I$ for $j=0$ and $j=10$, respectively.

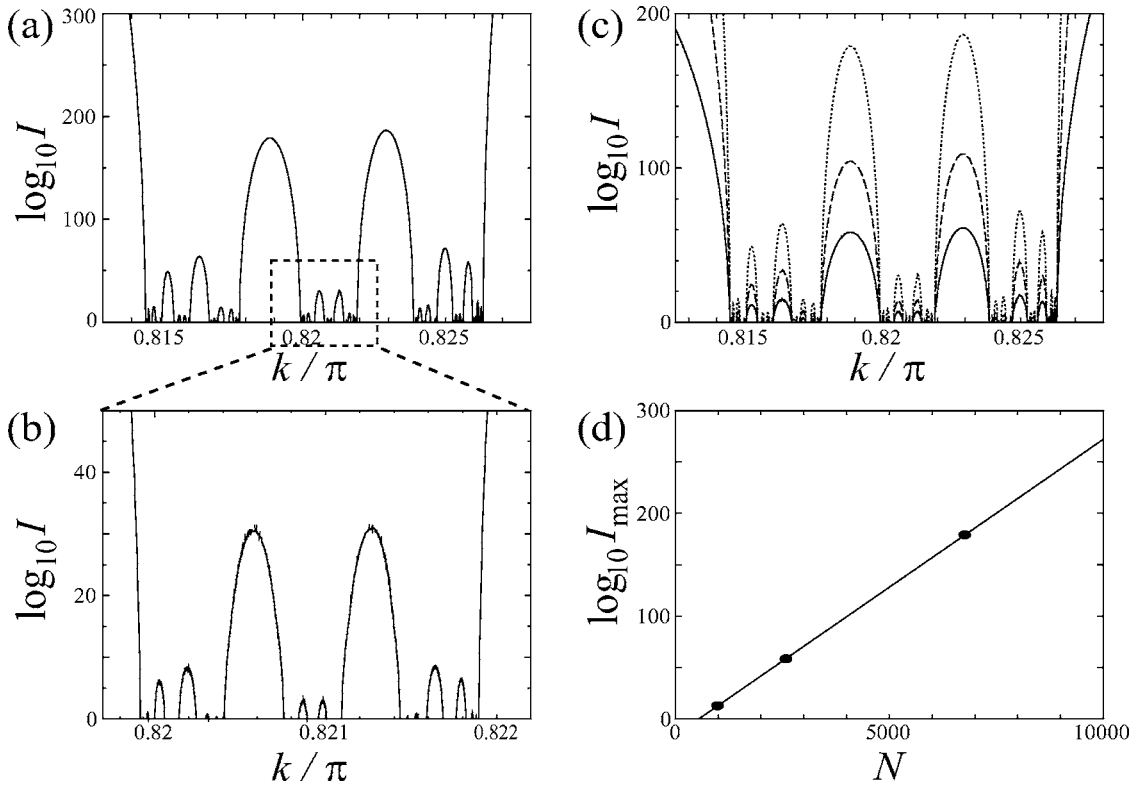

FIG. 9. Fractal-like behavior of $\log_{10} I$. (a) $\log_{10} I$ vs k/π in Fibonacci array of AB rings at $f=0.5\pi$, $a:b=1:3$. (b) The line shape of I-function in the enlarged region of $0.8197 \leq k/\pi \leq 0.8222$ in (a). (c) The solid line, the dashed line, and the dotted line are the line shapes of $\log_{10} I$ for $j=15$, $j=17$, and $j=19$, respectively. (d) $\log_{10} I_{\max}$ vs the number of AB rings N.

$j=0$ in the region of the transmission gaps. This remarkable discrepancy in the I-function behavior indicates that *the value of the function is independent of the generation number for* $|x_j| \leq 1$, *while the value of the function is dependent on the generation number for* $|x_j| > 1$. Thus, the I-function behavior is exhibited only for $|x_j| \leq 1$. Here, to distinguish between the transmission gap where the line shape of the I-function at $j=0$ approaches infinity and the region where the line shape of the function for $j \neq 0$ exhibits peaks in the region of the transmission gaps, we define the transmission gaps in the region of the transmission minibands as a transmission rift. These peaks of the line shape of the I-function imply that the transmission gaps are caused by breaking the time-reversal symmetry, and the transmission rifts are caused by the influence of the Fibonacci array of rings.

Figure 9(a) shows the line shape of the I-function as a function of k/π at $j=19$, and Fig. 9(b) is the line shape of the function in the enlarged region of $0.8197 \leq k/\pi \leq 0.8222$ in Fig. 9(a). As shown in Figs. 9(a) and 9(b), the line shape of the I-function suggests a *fractal-like behavior*. Figure 9(c) shows the line shape of the function as a function of k/π at $j=15$ (solid line), $j=17$ (dashed line), and $j=19$ (dotted line). The line shapes of the I-function in Fig. 9(c) show that as the generation number increases, the magnitude of the peak that appears within the transmission rifts increases. In addition, Fig. 9(d) shows the relationship between the maximum values of the peaks of the line shapes of the I-function and the number of AB rings corresponding to the Fibonacci number. The maximum values of the peak at $j=15$, 17, and 19 are fitted in a straight line (i.e., $I_{\max}$ at the wave number having the maximum value of the peaks increases exponentially as the Fibonacci number increases). Here, we are led to anticipate that the self-similarity feature emerging in the transmission rifts can be associated with the fractality of peaks of the I-function. Thus, in order to verify this behavior of the function, we introduce a quantity called the local maximum value, which is the height of each local peak of the common logarithm of the I-function within the transmission rift. We further divide the local maximum value by the system size N [see Fig. 9(d)]. Thus, the reduced local maximum value $\lambda_{\max}$ is defined as follows:

$$\lambda_{\max} \equiv \frac{1}{N} \log_{10} I_{\max}. \tag{18}$$

It is noted that Eq. (18) is applied in the region of k where the trace of the transmission probability exhibits transmission rifts. If the relationship between the local maximum value $\lambda_{\max}$ and the width of the transmission rift w_r exhibits a fractal behavior, a scaling law for the Fibonacci array of AB rings can be obtained.[41,42] In addition, the scaling index for the relationship between $\lambda_{\max}$ and w_r can be independent of the generation number.

Next, we investigate the relationship between the local maximum value $\lambda_{\max}$ and the width of the transmission rift w_r. Figure 10 shows (on a log-log scale) the relationship between the variation of $\lambda_{\max}$ and the width of the transmission rift w_r for several j. Figures 10(a) and 10(b) show the

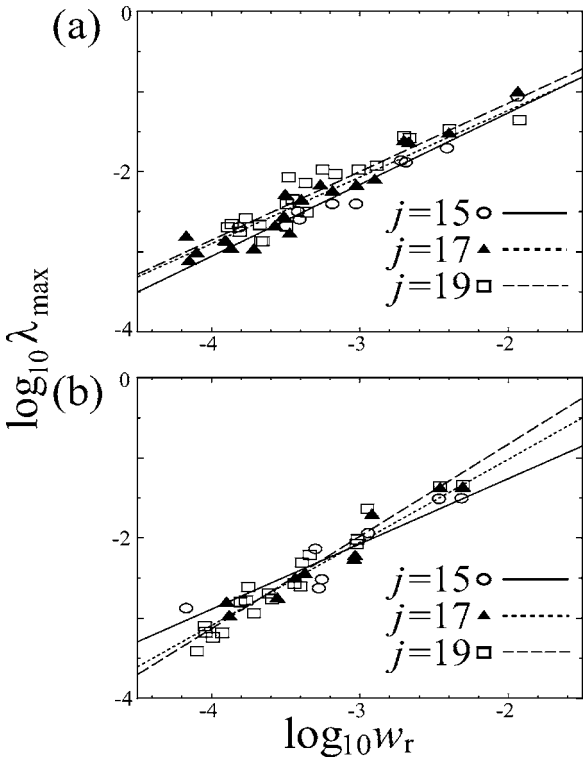

FIG. 10. The local maximum value λ_{max} vs the width of transmission rift w_r. The straight lines show least-square fits to the data for $j=15$ (solid line), $j=17$ (dotted line), and $j=19$ (dashed line). The ratio of units α and β are (a) $a:b=1:3$ and (b) $a:b=2:3$.

results of the least-squares fit to the data for (λ_{max}, w_r) with $a:b=1:3$ and $a:b=2:3$. The fits in Figs. 10(a) and 10(b) are represented by the solid ($j=15$), dotted ($j=17$), and dashed lines ($j=19$). The slopes of the lines α_R in Fig. 10(a) 0.894 ($j=15$), 0.830 ($j=17$), and 0.854 ($j=19$), while the slopes of the lines α_R in Fig. 10(b) are 0.814 ($j=15$), 1.04 ($j=17$), and 1.15 ($j=19$). From Fig. 10, we deduce that the relationship between λ_{max} and w_r is given by

$$\lambda_{max} \sim (w_r)^{\alpha_R}, \tag{19}$$

where the scaling index α_R is affected by the half-circumference and the number of AB rings corresponding to the generation number j. Therefore, we find that *the relationship between* λ_{max} *and* w_r *is characterized by the scaling law* (19) *in the Fibonacci array of AB rings*. In addition, the slope of the line (i.e., scaling index) for $j=15$ in Fig. 10(a) is in good agreement with those for $j=17$ and $j=19$, while the slope of the line for $j=15$ in Fig. 10(b) is in disagreement with those for $j=17$ and $j=19$. This correspondence of α_R indicates that the appearance of fractal behavior for the line shape of the I-function is closely related to the appearance of self-similarity for the trace of the transmission probability. Indeed, the trace of the transmission probability for $a:b=1:3$ exhibits self-similarity, while that for $a:b=2:3$ does not exhibit self-similarity. Therefore, we claim that *self-similarity appears in the trace of the transmission probability when* α_R *is in good agreement with* α_R *at another generation number, and it is essential to pick out the relevant parameters, which are the ratio of the half-circumferences of AB rings and the value of the magnetic flux number, to observe the self-similarity*. This correspondence of the scaling index at each generation number presents an approach for characterizing the self-similarity of the transmission probability. The invariant I proposed by Kohmoto *et al.* plays a pivotal role as a diagnostic tool in the study of electronic transport properties, notwithstanding its j dependency in our system concerned here.

IV. SUMMARY AND REMARKS

The property of electric transport in the Fibonacci array of 1D AB rings are studied by utilizing a transmission probability derived from the transfer matrix method and an invariant (I-function) derived from renormalization-group ideas. From the trace of transmission probability and I-function as a function of wave number, we have found the following characteristic features: (i) the expression for T_{F_j} in the Fibonacci array of rings is identical to the expression for T_S except for the half-circumference term, and the behavior of the transmission probability at $f=0$ is independent of the arrangement rule for rings. (ii) In the region of k which the line shape of I-function exhibits smooth curve approaching to zero at $f=0.5\pi$, six cycle for j appears in the traces of transmission probability regardless of the appearance of self-similarity formed by three bunch structures. Therefore the six cycle behavior for j is an intrinsic character of the transport property of Fibonacci arrays. (iii) The resonance points appear when the line shape of the I-function exhibits dips, while antiresonances (the transmission gaps) appear when the line shape of the I-function approaches infinity. (iv) The value of the I-function is independent of the generation number in the region of the transmission minibands, while the value of the I-function is dependent on the generation number within the transmission rift. (v) The line shape of the I-function within the transmission rift exhibits fractal-like behavior. (vi) The relationship between local maximum value and the width of transmission rift is characterized by scaling law, where the scaling index is affected by the half-circumference and the number of AB rings corresponding to the j. (vii) Self-similarity appears in the trace of the transmission probability when α_R is in good agreement with α_R at another generation number, and it is essential to pick out the relevant parameters, which are the ratio of the half-circumferences of AB rings and the value of the magnetic flux number, to observe the self-similarity.

There is a paper that demonstrated essential differences between a standard tight-binding model and a full continuous model.[8] In addition, Chakrabarti *et al.*[18] presented that in the quasiperiodic system of AB rings based on tight-binding model, the value of the invariant should not necessarily correspond to zeros at the energy that the resonance occurs. Thus, the relationship between the resonance and the vanishing of the I-function could be presented by an idealized model (a full continuous model) of AB rings.

In general, it will be necessary to take into account interactions such as electron-electron, spin-orbit, and electron-phonon in real AB ring systems. Indeed, studies on the inter-

actions have considered 1D aperiodic arrays.[43,44] It is attractive to study the effect of such interactions; however, the subject of our study is to elucidate the property of electronic transport controlled by the geometrical configuration of the AB rings according to the Fibonacci rule. Thus, we applied to the ideal 1D AB ring except for the interactions such as electron-electron, spin-orbit, and electron-phonon in our study.

We add some remarks. The magnetic flux number for $f \neq 0$ was fixed at 0.5π in our discussion. The reason why we fixed the magnetic flux number at $f=0.5\pi$ is as follows. In the case of $f=n_e\pi$ (n_e, an even number), Eqs. (3) and (4) correspond to the case of $f=0$. Thus, the transmission probability at $f=n_e\pi$ is identical to that at $f=0$, and besides, the trace of the transmission probability at $f=n_e\pi$ is independent of arrangement rule of rings. Meanwhile, Eq. (3) in the case of $f=n_o\pi$ (n_o, an odd number) becomes zero. The transmission probability in double AB rings when the wave number and half-circumference of the rings are fixed is given by $T_D=g(\cos f)\cos^4(f/2)/h(\cos f)$. Thus, the transmission probability at $f=n_o\pi$ becomes zero. As discussed in Sec. III, we found that the resonance and antiresonance state in double AB ring at $f=0.5\pi$ retain these states in the Fibonacci array of AB rings at $f=0.5\pi$. We consider that the resonance and antiresonance points at $f=\pi/2$ retain the same points for another f except for $f=n\pi$ (n, an even number). Therefore, these results indicate that the transmission probability at $f=\pi/2$ expresses the most effective transport properties affected by both the phase shift due to the external field and the multiple scattering at the nodal points for the arrangement of AB rings according to the Fibonacci rule.

In a previous study, there were features such as the stable and the transient gaps observed in the electronic spectra for the strongly modulated tight-binding Hamiltonian.[45] The features such as stable and transient gaps may coexist within the transmission rift in our model. In addition, the invariant (I-function) analysis obtained by the application of renormalization-group ideas in our study on the Fibonacci array of AB rings may be applicable to a 1D aperiodic system that is defined in terms of other inflation rules;[46,47] work along these lines is in progress.

ACKNOWLEDGMENTS

The authors are indebted to Mitsuhiro Akimoto and Akiyuki Iwaya for very useful comments besides critical reading of the paper.

*Electronic address: nomata@jan.rikadai.jp

[1] M. Kohmoto and J. R. Banavar, Phys. Rev. B **34**, 563 (1986).
[2] M. Kohmoto, B. Sutherland, and C. Tang, Phys. Rev. B **35**, 1020 (1987).
[3] M. Kohmoto, B. Sutherland, and K. Iguchi, Phys. Rev. Lett. **58**, 2436 (1987); W. Gellermann, M. Kohmoto, B. Sutherland, and P. C. Taylor, *ibid.* **72**, 633 (1994).
[4] T. Ninomiya, J. Phys. Soc. Jpn. **55**, 3709 (1986).
[5] S. Das Sarma and X. C. Xie, Phys. Rev. B **37**, 1097 (1988).
[6] F. Laruelle and B. Etienne, Phys. Rev. B **37**, 4816 (1988).
[7] Y. Avishai and D. Berend, Phys. Rev. B **41**, 5492 (1990).
[8] K. Moulopoulos and S. Roche, Phys. Rev. B **53**, 212 (1996).
[9] E. Maciá and F. Domínguez-Adame, Phys. Rev. Lett. **76**, 2957 (1996).
[10] (a) G. J. Jin, Z. D. Wang, S. S. Kang, and A. Hu, J. Phys. Soc. Jpn. **67**, 49 (1998); (b) G. J. Jin, Z. D. Wang, A. Hu, and S. S. Jiang, J. Appl. Phys. **85**, 1597 (1999).
[11] X. Yang, Y. Liu, and X. Fu, Phys. Rev. B **59**, 4545 (1999).
[12] S. Roche and K. Moulopoulos, Phys. Rev. B **61**, 6048 (2000).
[13] R. W. Peng, G. J. Jin, Mu Wang, A. Hu, S. S. Jiang, and D. Feng, J. Phys.: Condens. Matter **12**, 5701 (2000).
[14] X. Q. Huang, S. S. Jiang, R. W. Peng, and A. Hu, Phys. Rev. B **63**, 245104 (2001).
[15] Y. M. Liu. R. W. Peng, G. J. Jin, X. Q. Huang, M. Wang, A. Hu, and S. S. Jiang, J. Phys.: Condens. Matter **14**, 7253 (2002).
[16] R. W. Peng, X. Q. Huang, F. Qui, Mu Wang, A. Hu, S. S. Jiang, and M. Mazzer, Appl. Phys. Lett. **80**, 3063 (2002).
[17] S. Chattopadhyay and A. Chakrabarti, J. Phys.: Condens. Matter **16**, 313 (2004).
[18] A. Chakrabarti, R. A. Römer, and M. Schreiber, Phys. Rev. B **68**, 195417 (2003).
[19] A. Nomata, S. Horie, and A. Suzuki, J. Korean Phys. Soc. **46**, 666 (2005).
[20] Z. Liu and W. Zhang, Phys. Rev. B **72**, 134304 (2005).
[21] M. Kohmoto, L. P. Kadanoff, and C. Tang, Phys. Rev. Lett. **50**, 1870 (1983).
[22] E. Maciá, Rep. Prog. Phys. **69**, 397 (2006).
[23] R. A. Webb, S. Washburn, C. P. Umbach, and R. B. Laibowitz, Phys. Rev. Lett. **54**, 2696 (1985); S. Washburn, C. P. Umbach, R. B. Laibowitz, and R. A. Webb, Phys. Rev. B **32**, 4789 (1985).
[24] Jian-Bai Xia, Phys. Rev. B **45**, 3593 (1992).
[25] D. Mailly, C. Chapelier, and A. Benoit, Phys. Rev. Lett. **70**, 2020 (1993).
[26] D. Takai and K. Ohta, Phys. Rev. B **48**, 1537 (1993).
[27] P. S. Deo and A. M. Jayannavar, Phys. Rev. B **50**, 11629 (1994).
[28] C. Basu and B. Y. Gu, Physica B **215**, 344 (1995).
[29] J. Li, Z. Q. Zhang, and Y. Liu, Phys. Rev. B **55**, 5337 (1997).
[30] Z. Pan, C. D. Gong, M. H. Lung, and H. Lin, Phys. Rev. E **59**, 6010 (1999).
[31] W. Rabaud, L. Saminadayar, D. Mailly, K. Hasselbach, A. Benoît, and B. Etienne, Phys. Rev. Lett. **86**, 3124 (2001).
[32] S. Pedersen, A. E. Hansen, A. Kristensen, C. B. Sørensen, and P. E. Lindelof, Phys. Rev. B **61**, 5457 (2000).
[33] J. Yi, J. H. Wei, J. Hong, and S-I. Lee, Phys. Rev. B **65**, 033305 (2001); W. Park and J. Hong, *ibid.* **69**, 035319 (2004).
[34] *The Physics of Low-Dimensional Semiconductors*, edited by J. H. Davies (Cambridge University Press, Cambridge, 1998).
[35] S. Griffith, Trans. Faraday Soc. **49**, 345 (1953); **49**, 650 (1953).
[36] M. Büttiker, Y. Imry, R. Landauer, and S. Pinhas, Phys. Rev. B **31**, 6207 (1985); R. Landauer, Z. Phys. B: Condens. Matter **68**, 217 (1987).
[37] Y. Aharonov and D. Bohm, Phys. Rev. **115**, 485 (1959).

[38] N. Byers and C. N. Yang, Phys. Rev. Lett. **7**, 46 (1961).
[39] M. Büttiker, Y. Imry, and R. Landauer, Phys. Lett. **96A**, 365 (1983).
[40] We calculated numerically the "invariant" of different Fibonacci system studied by Jin *et al.* (Ref. 10) (T-stubs) with different generation numbers. The matrix elements of their fundamental matrices also have singularities on the k axis [see Eq. (3) of Ref. 10(a)]. For their system, the introduction of singularities has nothing to do with the breakdown of time-reversal symmetry. We observed the same kind of j dependency of I for their system (unpublished calculation).
[41] R. B. Capaz, B. Koiller, and S. L. A. de Queiroz, Phys. Rev. B **42**, 6402 (1990).
[42] M. T. Velhinho and I. R. Pimentel, Phys. Rev. B **61**, 1043 (2000).
[43] J. Vidal, D. Mouhanna, and T. Giamarchi, Phys. Rev. B **65**, 014201 (2001).
[44] J. R. Suárez, E. Vallejo, E. Carvajal, and O. Navarro, Phys. Status Solidi B **242**, 1759 (2005).
[45] Frédéric Piéchon, Mourad Benakli, and Anuradha Jagannathan, Phys. Rev. Lett. **74**, 5248 (1995).
[46] S. F. Cheng and G. J. Jin, Phys. Rev. B **65**, 134206 (2002).
[47] S. Sengupta, A. Chakrabarti, and S. Chattopadhyay, Phys. Rev. B **71**, 134204 (2005).